agronomy

MDPI

Article

Uncaria tomentosa-Loaded Chitosan Oligomers–Hydroxyapatite–Carbon Nitride Nanocarriers for Postharvest Fruit Protection

Alberto Santiago-Aliste [1], Eva Sánchez-Hernández [1], Laura Buzón-Durán [1,*], José Luis Marcos-Robles [2], Jesús Martín-Gil [1] and Pablo Martín-Ramos [1,*]

[1] Department of Agricultural and Forestry Engineering, ETSIIAA, University of Valladolid, Avenida de Madrid 44, 34004 Palencia, Spain; alberto.santiago@estudiantes.uva.es (A.S.-A.); eva.sanchez.hernandez@uva.es (E.S.-H.); jesus.martin.gil@uva.es (J.M.-G.)

[2] Department of Materials Science and Metallurgical Engineering, Engineering Graphics, Engineering Cartography, Geodesy and Photogrammetry, Mechanical Engineering and Manufacturing Process Engineering, ETSIIAA, University of Valladolid, Avenida de Madrid 44, 34004 Palencia, Spain; joseluis.marcos@uva.es

* Correspondence: laura.buzon@uva.es (L.B.-D.); pmr@uva.es (P.M.-R.)

Abstract: Given the risks associated with synthetic fungicides, it is crucial to explore safe and sustainable alternatives. One potential solution is using bioactive natural products (BNPs). However, BNPs face challenges like lability, solubility, and lack of specificity. These issues can be addressed through nanoencapsulation. This study focuses on the evaluation of novel chitosan oligomers–hydroxyapatite–carbon nitride (COS–HAp–g-C_3N_4) nanocarriers (NCs) for encapsulating BNPs, specifically an extract from *Uncaria tomentosa* bark. The NCs were characterized by transmission electron microscopy, energy-dispersive X-ray spectroscopy, and infrared spectroscopy. The NCs were monodisperse, with a mean diameter of 250 nm, and showed an encapsulation efficiency of 82%. The suitability of the loaded NCs (COS–HAp–g-C_3N_4–BNP, in a 2:1:0.5:1 weight ratio) for postharvest fruit protection was investigated in vitro and ex situ at a laboratory scale. Results regarding their efficacy against *Botrytis cinerea* on strawberries, *Colletotrichum gloeosporioides* on mangoes, *Penicillium expansum* on apples, *Monilinia laxa* on peaches, and *Sclerotinia sclerotiorum* on kiwifruit are presented. Minimum inhibitory concentrations of 250, 375, 375, 250, and 187.5 μg·mL^{-1} were found in vitro, respectively, while higher doses (500, 750, 750, 250, and 375 μg·mL^{-1}, respectively) were needed to achieve effective control in postharvest tests on artificially inoculated fruit. These findings suggest that NCs containing extracts from *U. tomentosa* bark show promise as biorational agents and as alternatives to conventional fungicides for managing postharvest phytopathogens.

Keywords: cat's claw; biopolymeric nanoparticles; chitosan oligomers; g-C_3N_4; nanoencapsulation; natural fungicides; postharvest fruit diseases; stimuli-responsive systems; shelf-life extension; sustainable crop protection

Citation: Santiago-Aliste, A.; Sánchez-Hernández, E.; Buzón-Durán, L.; Marcos-Robles, J.L.; Martín-Gil, J.; Martín-Ramos, P. *Uncaria tomentosa*-Loaded Chitosan Oligomers–Hydroxyapatite–Carbon Nitride Nanocarriers for Postharvest Fruit Protection. *Agronomy* **2023**, *13*, 2189. https://doi.org/10.3390/agronomy13092189

Academic Editor: Prakash M Gopalakrishnan Nair

Received: 7 August 2023
Revised: 18 August 2023
Accepted: 20 August 2023
Published: 22 August 2023

1. Introduction

Nanocarriers (NCs) have been studied in recent decades due to their potential in drug delivery. Their high surface-area-to-volume ratio enables them to modify the fundamental characteristics and bioactivity of drugs. Nanocarriers offer various benefits, including enhanced pharmacokinetics and biodistribution, reduced toxicities, improved solubility and stability, a controlled release, and the targeted delivery of therapeutic agents [1]. In the field of medical microbiology, NCs are considered a promising strategy for combating multidrug resistance in fungi [2].

Beyond medical applications, NCs are also gaining attention in agriculture and food packaging. In agriculture, NCs show promise in developing new bioactive product formulations. Incorporating antimicrobials into NCs offers benefits such as increased surface

area for interaction, improved solubility and absorption, protection against environmental stresses, and a targeted, controlled release. Various types of NCs have been explored for crop protection, such as nanocapsules, nanospheres, micelles, and nanogels [3]. Concerning NC composition, inorganic materials like mesoporous silica, carbon-based nanomaterials (e.g., graphene oxide), clay minerals, metal–organic frameworks (MOFs), calcium carbonate, boron nitride, and MXenes have been successfully tested. These materials offer advantages for the loading of active ingredients due to their high specific surface area and porosity, ease of surface functionalization and hydrophobicity adjustment, and pore size structure for a sustained/controlled release [4]. Synthetic polymer- (e.g., poly(lactic acid), polydopamine, and polyurethane), lipid- (nanoemulsions, nanoliposomes, and solid lipid nanoparticles), cyclodextrin-, and biopolymeric-based NCs (proteins, lignin, and polysaccharides) are popular alternatives [5]. The latter are particularly attractive due to their renewable nature, edibility, environmental-friendliness, and production flexibility. Reviews by Xiao et al. [4], Pinto et al. [6], Tao et al. [7], and Zhou et al. [8] offer insights into stimuli-responsive systems for the delivery of agrochemicals.

Regarding the encapsulated active ingredients, conventional fungicides are the predominant choice, as discussed in the review by Tleuova et al. [9]. The review by Fincheira et al. [10] has addressed the application of controlled release systems for agrochemicals beyond pesticides, such as fertilizers, contributing to the eco-efficiency of the system and enabling smart agriculture. In the food industry, NCs loaded with natural antimicrobial agents (including essential oils (EOs), antimicrobial peptides, and organic acids) have garnered significant attention in active packaging [5]. The recent review by Yang et al. [11] comprehensively covers the utilization of chitosan NCs for encapsulating EOs, encompassing antimicrobial applications that primarily involve antibacterial activity, along with some instances of antifungal activity.

In this study, we present NCs formed by combining chitosan oligomers (COS) as a biopolymer, hydroxyapatite (HAp), and carbon nitride (g-C_3N_4) as an inorganic 2D material. These NCs build upon the multifunctional COS–g-C_3N_4 NCs that were previously reported by our group [12]. Chitosan was selected for its film-forming ability, biodegradability, biocompatibility, antimicrobial properties, and pH-responsiveness. The inclusion of g-C_3N_4 contributes to bioactive product delivery by offering low toxicity, excellent biocompatibility, high tissue penetration, photosensitivity, pH sensitivity, efficient drug encapsulation (due to its large surface area), and a positive effect on release [13]. Additionally, incorporating HAp is justified by its biodegradability, biocompatibility, and bioactivity in the human body. HAp has successfully served as a delivery agent for antibiotics, anticancer drugs, nucleic acids, and proteins, benefitting from its high surface-area-to-volume ratio and surface activity. Moreover, considering the successful demonstration of chitosan-coated HAp NCs for curcumin delivery by Hemmati et al. [14], the investigation of a syncretic system comprising the COS–HAp–g-C_3N_4 assembly proves to be an intriguing avenue for further research. Regarding the bioactive product to be encapsulated, *Uncaria tomentosa* (Willd. ex Schult.) DC bark extract was chosen due to its potent fungicidal activity, which is comparable to conventional fungicides [15].

The primary objective of this research has been to characterize the COS–HAp–g-C_3N_4 NCs and evaluate the efficacy of *U. tomentosa*-extract-loaded NCs, both in vitro and ex situ, for providing postharvest protection to fruits. The bioactivity assessment involved five economically significant phytopathogens: *Botrytis cinerea* Pers. (grey mold) on strawberries, *Colletotrichum gloeosporioides* (Penz.) Penz. & Sacc. (anthracnose) on mangoes, *Penicillium expansum* Link (blue mold) on apples, *Monilinia laxa* (Aderh. & Ruhland) Honey (brown rot) on peaches, and *Sclerotinia sclerotiorum* (Lib.) de Bary (sclerotinia rot) on kiwifruit. Among these, *B. cinerea* and *Colletotrichum* spp. ranked second and eighth, respectively, on a list of scientifically and economically important fungal pathogens [16]. *Botrytis cinerea* has a broad host range (over 200 plant species) and can cause severe damage preharvest and postharvest, while *C. gloeosporioides* leads to significant economic losses in fruit and vegetable crops in preharvest and postharvest stages, particularly in tropical and subtropical climates [17].

Penicillium expansum is a major apple pathogen responsible for significant economic losses after harvest, producing patulin, a harmful mycotoxin to humans [18]. *Monilinia laxa* causes substantial losses in stone fruit both in the field and after harvest (up to 80% of fruit loss), with estimated annual losses of 1.7 billion Euros globally [19,20]. *Sclerotinia sclerotiorum* affects flowers, shoots, leaves, developing fruits, and stored kiwifruit [21,22].

Given the significance and wide-ranging impact of these selected pathogens, the findings presented in this study have the potential to make valuable contributions to the sustainable management of postharvest diseases. This research can offer benefits not only to the tested fruits but also to other crops affected by similar fungal taxa.

2. Material and Methods

2.1. Reagents and Fungal Isolates

High-molecular-weight chitosan (CAS 9012-76-4) came from Hangzhou Simit Chem. & Tech. Co. (Hangzhou, China). Neutrase^{TM} 0.8 L enzyme was supplied by Novozymes A/S (Bagsværd, Denmark). Melamine cyanurate (CAS 37640-57-6; >99.0%) was purchased from Nachmann S.r.l. (Milano, Italy). Chitosanase from *Streptomyces griseus* (Krainsky) Waksman and Henrici (EC 3.2.1.132, CAS 51570-20-8), acetic acid (CAS 64-19-7; purum, 80% in H_2O), methacrylic anhydride (CAS 760-93-0; ≥94%), calcium hydroxide (CAS 1305-62-0; 99.995% trace metals basis), phosphoric acid (CAS 7664-38-2; ACS reagent, ≥85 wt. % in H_2O), methanol (UHPLC, suitable for mass spectrometry, CAS 67-56-1), tetrahydrofuran (THF, CAS 109-99-9; ≥99.9%), and Tween® 20 (CAS 9005-64-5) were obtained from Merck (Darmstadt, Germany). Ammonium hydroxide solution (CAS 1336-21-6, 50% *v*/*v* aq. soln.) was supplied by Alfa Aesar (Ward Hill, MA, USA). Becton, Dickinson, and Company (Franklin Lakes, NJ, USA) supplied the potato dextrose broth (PDB) and potato dextrose agar (PDA).

For in vitro experiments, several fungicides served as positive controls: Ortiva® (azoxystrobin 25%; Syngenta, Basel, Switzerland), Vondozeb® (mancozeb 75%; UPL Iberia, Barcelona, Spain), and Fesil® (fosetyl-Al 80%, Bayer, Leverkusen, Germany), courtesy of the Plant Health and Certification Center of the Gobierno de Aragón (Zaragoza, Spain).

Botrytis cinerea (CECT 20973), *C. gloeosporioides* (CECT 21107), and *P. expansum* (CECT 20906) originated from the Spanish Type Culture Collection (Valencia, Spain). *Monilinia laxa* (MYC-1580) and *S. sclerotiorum* (MYC-799) were provided by the Mycology lab at the Center for Research and Agrifood Technology of Aragón (Zaragoza, Spain) as subcultures on PDA.

2.2. Plant Material and Preparation of Extract

The *U. tomentosa* specimens for preparing the BNP to be encapsulated were gathered in La Merced (Chanchamayo, Peru).

The fruits used in the ex situ bioassays (specifically, strawberry cv. 'Fortuna', mango cv. 'Keitt', apple cv. 'Golden Delicious', peach cv. 'Summer sun', and kiwifruit cv. 'Hayward Green') were provided by Tienda Ecológica Madrid–Almanatur (El Viso de San Juan, Toledo, Spain). They were all grown organically, adhering to organic farming regulations. The fruits were selected based on uniform size, and absence of physical damage and fungal infections, and were shipped respecting the cold chain. The cultivars were chosen due to their widespread availability to consumers in Spain.

2.3. Chitosan Oligomers, g-C_3N_4, and Hydroxyapatite Preparation

Chitosan oligomers and high-purity nanosheets of g-C_3N_4 were prepared following the previously described procedure for COS–g-C_3N_4 NCs [12]. Briefly, the preparation of COS mostly followed the process outlined in [23], utilizing citric acid to dissolve the high-MW chitosan (310–375 kDa) under constant stirring at 60 °C. Neutrase^{TM} was then used to degrade the chitosan, obtaining—via sonication with a model UIP1000hdT probe-type ultrasonicator (Hielscher Ultrasonics; Teltow, Germany)—a solution of oligomers of MW in the 3-to-6 kDa range, with a polydispersity index of 1.6. Nanosheets of g-C_3N_4 were obtained

via pyrolysis at 600 °C of melamine cyanurate under air atmosphere for 50 min [24]. To obtain fine HAp powder particles, a solution of H_3PO_4 with $Ca(OH)_2$ was used, following the procedure described in [25] with slight modifications in the ultrasonication conditions.

2.4. Synthesis of the COS–HAp–g-C_3N_4 Nanocarriers

The preparation of the NCs was performed as described in the Spanish patent application P202330435. The three constituents were initially modified with methacrylic anhydride (MA). The synthesis of methacrylated chitosan was conducted according to the procedure proposed by Gupta and Gupta [26], with modifications (employing COS instead of chitosan and MA instead of epichlorohydrin as a cross-linking agent). In short, 420 mg of oligomers were added to a solution of 0.5 mL MA in 25 mL of THF, followed by ultrasonication for 30 min (in 10 min intervals, alternated with 5 min intervals without sonication). The methacrylation of HAp was performed by dispersing 210 mg of HAp in a solution of MA in THF (0.25 mL in 12.5 mL) and subjecting it to ultrasonication. As for the third co-encapsulating chemical species, the procedure was analogous, starting from 105 g of g-C_3N_4.

The methacrylated HAp solution was then slowly added to the methacrylated COS solution, followed by ultrasonication and stirring for 30 min. Subsequently, the methacrylated g-C_3N_4 solution was also added gradually to this mixture, followed by ultrasonication and stirring. The resulting solution was further stirred for 24 h, centrifuged, repeatedly washed with milli-Q water to remove excess MA, and freeze-dried, resulting in a COS:HAp:g-C_3N_4 weight ratio of 2:1:0.5. Higher weight ratios of g-C_3N_4 did not yield nanosphere formation, and alternative COS:HAp weight ratios led to non-monodisperse size distributions.

2.5. Encapsulation and Release of U. tomentosa Extract

The *U. tomentosa* bark's aqueous ammonia extract preparation, along with its characterization using gas chromatography–mass spectroscopy, was previously reported in [15].

To prepare NCs containing the *U. tomentosa* extract, 210 mg of the lyophilized extract to be encapsulated were redissolved in methanol and added to the COS–HAp–g-C_3N_4 NCs solution, resulting in a COS:HAp:g-C_3N_4:*U. tomentosa* weight ratio of 2:1:0.5:1. The mixture was sonicated for 1 h in 10 min intervals while maintaining a temperature below 60 °C and a pH of 4–5.

Regarding the encapsulation efficiency (EE) of the plant extract, it was determined using Fischer et al.'s indirect method [27]: the sample underwent centrifugation at 10,000 rpm (1 h), and the supernatant containing the non-encapsulated extract was freeze-dried, redissolved in methanol, filtered through a 0.2 µm filter, and analyzed using high-pressure liquid chromatography (HPLC) with an Agilent 1200 series system (Agilent Technologies; Santa Clara, CA, USA). The operating conditions were as follows [28]: mobile phase of methanol-5% acetic acid (pH 3) (70~30), injection volume of 10 µL, column temperature of 20 °C, flow rate of 0.2 mL·min^{-1}, and detection at 250 nm using the G1315D detector. The encapsulation efficiency (EE) was determined as $EE(\%) = ((m_{extract\ initial} - m_{extract\ supernatant})/m_{extract\ initial}) \times 100$. An average EE across 10 repetitions is reported.

For the release efficiency (RE), release assays (n = 10) were conducted by adding a weighed amount of freeze-dried loaded NCs (obtained from the encapsulation efficiency test) and 2.5 U of chitosanase (EC 3.2.1.132) to a methanol:water (1:1, v/v) solution under light stirring (150 rpm) in the dark for 2 h. An aliquot was sampled, and the released *U. tomentosa* extract was processed using the same methodology explained earlier for determining the residual (non-encapsulated) extract. The release efficiency was calculated as the percentage of the released extract relative to the total amount of extract encapsulated in the NCs.

2.6. Nanocarrier Characterization

Transmission electron microscopy (TEM) characterization was performed using a JEM 1011 HR microscope (JEOL; Tokyo, Japan) at 100 kV and 25,000–120,000× magnification.

Micrographs were obtained with a GATAN ES1000W CCD camera (4000 × 2672 pixels). Negative staining of the samples was performed using 2% uranyl acetate. The polydispersity was calculated from TEM data as $p = \sigma/R_{avg}$, where p is the polydispersity index, σ is the standard deviation of the radius in a batch of NCs, and R_{avg} is the average radius of the NCs [29].

The multi-elemental composition of the NCs, before and after loading with the BNP (*U. tomentosa* extract), was analyzed by scanning electron microscopy with energy-dispersive X-ray spectroscopy (SEM–EDS) using an EVO HD 25 (Carl Zeiss; Oberkochen, Germany) apparatus.

Vibrational spectra were collected using a Nicolet iS50 Fourier-transform infrared (FTIR) spectrometer (Thermo Scientific; Waltham, MA, USA) equipped with a diamond attenuated total reflection (ATR) system. Spectra were recorded in the range of 400–4000 cm^{-1} with a spectral resolution of 1 cm^{-1}, and the interferograms resulting from the co-addition of 64 scans were saved.

The phase composition of the samples was characterized using a D8 Advance diffractometer (Bruker; Billerica, MA, USA), equipped with Cu Kα X-ray source (λ = 0.15406 nm). The X-ray powder diffraction (XRPD) pattern was recorded in the 2θ = 5–70° range.

2.7. In Vitro Antimicrobial Activity

The antifungal activity of the COS–HAp–g-C_3N_4 NCs, both before and after encapsulation of *U. tomentosa* extract, along with that of non-encapsulated extract (for comparison), was determined using the poisoned food method following the EUCAST antifungal susceptibility testing standard procedures [30]. Stock solutions of the *U. tomentosa* extract and the NCs, whether empty or loaded with the BNP, were incorporated into a PDA medium to achieve concentrations ranging from 62.5 to 1500 $\mu g \cdot mL^{-1}$. Fungal mycelium plugs were transferred from the margins of 1-week-old PDA cultures of *B. cinerea*, *C. gloeosporioides*, *M. laxa*, and *S. sclerotiorum*, as well as a 2-week-old culture of *P. expansum*, to plates containing the specified concentrations for each treatment. Three plates per treatment/concentration combination were prepared, with two replicates each. Incubation was conducted under specific conditions for each fungus: *B. cinerea*, *C. gloeosporioides*, and *S. sclerotiorum* plates were incubated at 25 °C in the dark for 1 week, and *P. expansum* for 2 weeks. In the case of *M. laxa*, incubation was carried out at 22 °C in the dark for 1 week. The untreated control consisted of pure PDA medium. Positive controls utilized commercial fungicides (Ortiva®, Vondozeb®, and Fesil®) at the doses recommended by each manufacturer.

The radial growth of the mycelium was evaluated by measuring the average of two colony diameters that were perpendicular to each other for each repetition. Growth suppression was determined using the formula $((d_c - d_t)/d_c) \times 100$, where d_c and d_t represent the mean colony diameter of the untreated control and the treated fungus, respectively. Effective concentrations (ECs) were estimated by fitting a four-parameter logistic equation (dose–response curve). Synergy factors (SFs) were estimated from effective concentration values using Wadley's method, assuming a ca. 25% BNP weight ratio [31], based on the EE results.

2.8. Preparation of Fungal Conidial Suspension

Fungal conidial suspensions were prepared as described in [32]. Conidia were obtained from 1-week-old PDB cultures of *C. gloeosporioides*, *M. laxa*, and *S. sclerotiorum*, as well as from a 2-week-old PDB culture of *P. expansum*. After filtration through two layers of sterile muslin to remove somatic mycelia, the spore concentration was determined using a hemocytometer and adjusted to 1×10^6 spores (conidia)$\cdot mL^{-1}$.

2.9. Ex Situ Protection of Commercial Fruits

The efficacy of the COS–HAp–g-C_3N_4 NCs loaded with the BNP (*U. tomentosa* extract) for postharvest protection of strawberry fruits infected with *B. cinerea* was evaluated as

proposed in [15]. Strawberries were disinfected for 2 min with a 3% NaOCl solution, then washed three times with sterile distilled water, and dried in a laminar flow hood on sterile absorbent paper. Strawberries were randomly distributed into four homogeneous groups of 45 fruits each (three replicates with 15 fruits per replicate and treatment). Two groups were treated with COS–HAp–g-C_3N_4–BNP NCs at different concentrations (MIC and MIC × 2, i.e., 250 and 500 μg·mL^{-1}, supplemented with 0.2% Tween® 20). The other groups served as negative (untreated and without pathogen) and positive (with pathogen and without treatment) controls. Then, 5 mm superficial wounds were made in the equatorial zone of each fruit, and the strawberries were immersed in the treatment for 5 min and dried at room temperature in a laminar flow hood using sterile absorbent paper. A plug of a 1-week-old PDA culture of *B. cinerea* (with the mycelium facing the fruit wound) was placed in the surface wounds. The fruits were then stored in covered plastic boxes for 7 days at 4 °C and 95–98% RH, followed by a 4-day storage period at 25 °C and 95–98% RH, after which lesion diameters (LDs) were measured on the fruit surfaces.

The efficacy of COS–HAp–g-C_3N_4–BNP treatment in postharvest protection of other fruits, namely, mango, peach, apple, and kiwifruit, artificially infected with *C. gloeosporioides*, *M. laxa*, *P. expansum*, and *S. sclerotiorum*, respectively, was also evaluated under controlled laboratory conditions, following the procedure indicated in [33]. The surface disinfection procedure and experiment design (involving four groups of 24 fruits each, i.e., three replicates with 8 fruits per replicate and treatment) were similar to those described above for strawberries, with one group treated with COS–HAp–g-C_3N_4–BNP NCs at a concentration equal to the MIC determined in vitro (375, 250, 375, and 187.5 μg·mL^{-1}, respectively), another group treated at twice the MIC (750, 500, 750, and 375 μg·mL^{-1}, respectively), and negative and positive controls. However, the inoculation procedure differed: under aseptic conditions, each fruit was punctured at two equidistant points in the equatorial region using a truncated needle (3 mm diameter × 5 mm depth), except for mangoes, to which two punctures were made on each side of the fruit. The punctures in the treated fruits were first filled with 20 μL of the corresponding treatment (at MIC or MIC × 2 concentration, supplemented with 0.2% Tween® 20). After 1 h, wounds were inoculated with 20 μL of a fungal pathogen spore suspension. Positive controls were inoculated only with the spore suspension, while negative controls were inoculated with sterile deionized water containing 0.2% Tween® 20. Each treatment was placed in a separate clean container with sterile moistened cotton and incubated at 25 °C and 95–98% RH for 4 days for peaches, 7 days for mangoes, 10 days for kiwifruits, and 15 days for apples, after which LDs were measured on the fruit surfaces.

In all cases, the lesion size reduction (LSR) percentage was calculated using the formula LSR (%) = $[(LD_c - LD_t)/LD_c] \times 100$, where LD_c and LD_t represent the mean lesion diameters of the positive control and the treated fruits, respectively. At the end of each experiment, the fruits were cut open to analyze their internal lesions.

It is important to note that a contrast fungicide was not used in these experiments because the Spanish national legislation on registration of phytosanitary products currently does not authorize fungicides for postharvest protection of strawberries, mangoes, and kiwifruit. Only pyrimethanil (19.2% *w*/*v*) + clove EO (18.5% *w*/*v*) is allowed for peaches, whereas thiabendazole 50% *w*/*v* is authorized for apples (although a resistance risk management strategy should be implemented, in accordance with Fungicide Resistance Action Committee recommendations).

2.10. Statistical Analysis

The mycelial growth inhibition results for the extract, the empty NCs, and the loaded NCs were evaluated using IBM SPSS Statistics v.25 (IBM; Armonk, NY, USA) through the Kruskal–Wallis non-parametric test, with Conover–Iman test for post hoc multiple pairwise comparisons (provided that the normality and homoscedasticity requirements were not met; Table S1). Mycelial growth inhibition results for the conventional fungicides were not subjected to statistical analysis as the assayed doses (recommended by the manufacturers)

were not comparable. A one-way analysis of variance (ANOVA), followed by Tukey's test for post hoc comparison of means, was employed to compare the efficacy of the treatments in the ex situ assays, given that, in this case, homogeneity and homoscedasticity were confirmed with the Shapiro–Wilk and Levene tests, respectively (Table S2).

3. Results

3.1. Nanocarrier Characterization

3.1.1. TEM Characterization

Upon characterization by TEM microscopy, the COS–HAp–g-C_3N_4 NCs appeared as perfect spheres when empty (Figure 1a), while those loaded with the BNP showed a slightly more irregular contour (Figure 1b). The encapsulation of the BNP did not significantly alter the NC size, which exhibited a log-normal distribution with mean diameters of 241.3 ± 74.3 nm and 266.5 ± 94.4 nm (10.4% higher) for the empty NCs and the NCs loaded with the *U. tomentosa* extract, respectively. The polydispersity index values (p_{empty} = 0.308 and p_{loaded} = 0.354, respectively), close to the acceptable 0.3 value for drug delivery applications using NCs, along with the presence of a single peak in the size distribution curve (Figure 1c), suggest the NCs' monodispersity [34].

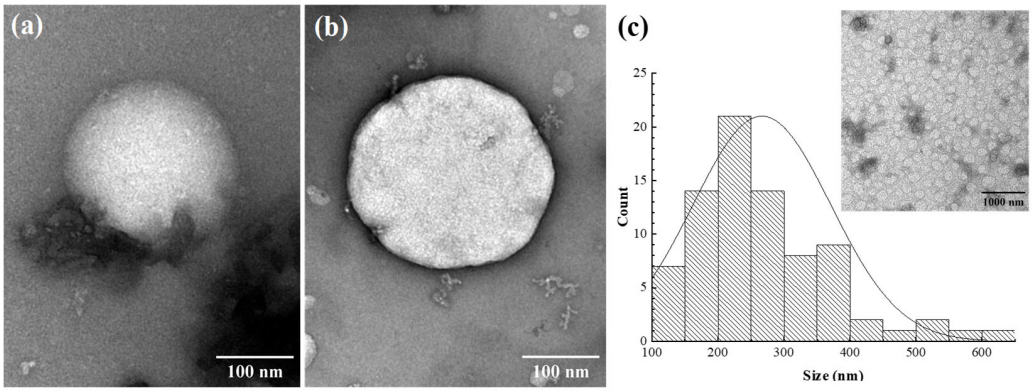

Figure 1. TEM micrographs of (**a**) an empty COS–HAp–g-C_3N_4 nanocarrier (NC) and (**b**) a COS–HAp–g-C_3N_4 NC loaded with *Uncaria tomentosa* extract. Uranyl acetate 2% staining was used as a negative-staining solution. (**c**) Size distribution histogram of NCs (n = 80). The inset illustrates the NCs in the field of view.

3.1.2. EDS Multi-Elemental Analysis

EDS analysis of the unfilled COS–HAp–g-C_3N_4 NCs (Figure S1a), utilizing the standardless ZAF quantification method, yielded the following atomic percentages: 41.96% C, 12.29% N, 40.49% O, 2.56% P, and 2.70% Ca. Assuming the molecular formulae of chitosan oligomers, hydroxyapatite, and carbon nitride (melem) to be $C_{56}H_{103}N_9O_{39}$, $Ca_{10}(PO_4)_6(OH)_2$), and $C_{60}N_{91}H_{33}$, respectively, and considering the use of 420, 210, and 105 mg in the synthesis, respectively, the calculated atomic percentages would be 40.95% C, 15.90% N, 35.76% O, 2.77% P, and 4.62% Ca. Consequently, the experimental data, albeit semi-quantitative, were sufficiently close to the expected values, supporting the idea that the component ratio for the unfilled COS–HAp–g-C_3N_4 assembly would be relatively close to the desired 2:1:0.5 weight ratio.

The results for the NCs filled with *U. tomentosa* extract showed atomic percentages of 38.51% C, 10.83% N, 34.32% O, 5.98% P, and 10.36% Ca (Figure S1b). Considering the same molecular formulae and starting weights mentioned above for the NC components, and attributing the composition of the BNP only to its main component, octyl isobutyrate, along with assuming a high encapsulation efficiency of the BNP (approximately 82% of the starting 210 mg, as discussed below), the expected atomic percentages would be: 50.36% C, 12.55% N, 31.24% O, 2.19% P, and 3.65% Ca. While the atomic percentages of N and O were somewhat close to the expected values, the atomic percentages of C, P, and Ca significantly

deviated from the expected values. Such discrepancies should be tentatively attributed to the semi-quantitative nature of the EDS data and the oversimplification of considering the BNP as pure octyl isobutyrate, given that this compound represents only 30.7% of the extract [15].

3.1.3. Infrared Vibrational Analysis

The infrared spectra of the empty COS–HAp–g-C_3N_4 NCs and the NCs loaded with the BNP are presented in Figure S2. Table 1 summarizes the main bands and their assignments.

Table 1. Main bands in the infrared spectrum of the pure COS–HAp–g-C_3N_4 nanomaterial (empty NCs) and after encapsulation of the bioactive natural compound (BNP), namely, *U. tomentosa* extract. Wavenumbers are expressed in cm^{-1}.

COS–HAp–g-C_3N_4	COS–HAp–g-C_3N_4–BNP	Assignment
3346	3327	NH_2 of CN heterocycles (*g*-C_3N_4)
3258	3201	N–H in COS–HAp assembly
2953	2924	ν(C–H) in alkyls (CH_2 and CH_3)
2839	2853	ν(C–H) in alkyls (CH and CH_3) from BNP esters
	1659	δ(N–H)
1640		ν(C=O) amide (methacrylation remains)
1610	1598	aromatic ring deformation (COS)
1564		C=O (COS)
1539		ν(C=C) alkenyl; δ(NH)+ν(C–N) in amides
1466	1452	$\nu_{as}(COO^-)$, isobutyrate
1423	1413	–NHCO amide; ν(C–H); δ(OH); ν_s(C=O) in COO^-
1389		$\nu(C–N^+)$; ν(C–H) in CH_3 groups
	1335	aliphatic CH_x
1308	1316	ν(C–N)
1266	1237	ν(C–N) (characteristic of g-C_3N_4)
1199	1206	characteristic of g-C_3N_4
1154	1151	$\nu_3(PO_4^{3-})$ of HAp; ν(C–N) amine (typical of COS)
1083		C=O of secondary hydroxyl groups (COS)
1018	1031	ν(C–O–C), saccharide in COS; C–N from amine
944	952	phosphate of HAp
919		C–O stretching
889	890	δ(C=C) or δ(N–H), tris-*s*-triazine (g-C_3N_4)
840	865	=C–H wagging (COS)
800	811	C–C axial stretching/tris-*s*-triazine (g-C_3N_4) breathing
595	599	bending vibration of O–P–O phosphate of HAp
561	560	bending vibration of O–P–O phosphate of HAp

The presence of the COS component in the COS–HAp–g-C_3N_4 assembly is evident from the peaks at 1564 cm^{-1} (C=O), the band at 1389 cm^{-1} (–NHCO of amide), and the band at 1031–1018 cm^{-1} (C–O–C group, saccharide structure).

The distinctive peaks at 560, 595–599, and 952 cm^{-1} (and perhaps also that at 1151 cm^{-1}) are attributed to the PO_4^{3-} of HAp (the peaks at 560 and 1151 cm^{-1} refer to the bending and symmetric stretching vibrations of P–O bonds, respectively).

Attributed to *g*-C_3N_4 are the bands at 3346–3327, 2853–2839, 1610–1598, 1237, 1206, 890, and 811 cm^{-1}. The band at 3336 cm^{-1} corresponds to the stretching vibrations of uncondensed primary (–NH–) amines present in residual amino groups on the edges of CN heterocycles. Multiple absorption peaks in the 1640–1200 cm^{-1} region can be associated with the C–N and C=N stretching vibrations of the CN aromatic repeating unit. The bands at 890 and 811 cm^{-1} correspond to the N–H deformation mode and the bending/breathing vibration mode of the g-C_3N_4 tri-*s*-triazine unit rings, respectively.

The spectrum of the NCs filled with *U. tomentosa* extract (Figure S2b) showed additional bands attributable to the presence of octyl isobutyrate (the main BNP component),

such as the one at 1450 cm^{-1}. The peak at 1659 cm^{-1} could be due to the N–H group deformation, indicating the interaction of the BNP with the COS–HAp–g-C_3N_4 assembly [13].

3.1.4. X-ray Powder Diffraction

The XRPD pattern of the freeze-dried COS–HAp–g-C_3N_4 NCs is depicted in Figure S3a. The weak peaks at $2\theta = 21^\circ$ and 23° can be attributed to the (102) and (022) reflections of COS (JCPDS Card No. 39-1894). The low crystallinity should be attributed to the freeze-drying procedure, as reported by Jaworska et al. [35]. The peaks at $2\theta = 25.8^\circ$, 31.7°, 32.1°, 32.9°, 46.0°, and 49.4° correspond to the reflection planes (002), (211), (112), (300), (312), and (213), respectively, of HAp (JCPDS Card No. 09–0432). Regarding the peaks at $2\theta = 13^\circ$ and 28°, they correspond to the (100) and (002) reflections, respectively, associated with the in-plane structural packing motif of the tris-*s*-triazine units and the interlayer stacking of g-C_3N_4 (JCPDS Card No. 87–1526). The slight shift towards higher angles indicates a tightening of the interplanar distance and stronger interplanar interaction [36]. The XRPD pattern of the BNP-loaded COS–HAp–g-C_3N_4 (Figure S3b) was similar, albeit more amorphous.

3.1.5. Encapsulation and Release Efficiencies

A moderate to high encapsulation efficiency of the BNP in the COS–HAp–g-C_3N_4 NCs was observed (EE = 82 ± 5%, n = 10). The release efficiency upon exposure of the NCs to a commercial chitosanase (EC 3.2.1.132) was high, ranging from 84% to 89% (n = 10).

3.2. Antifungal Activity

3.2.1. In Vitro Antifungal Activity

The results from the mycelial growth inhibition tests are depicted in Figure 2. The selected BNP, namely, *U. tomentosa* bark extract, demonstrated higher efficacy against *B. cinerea* (MIC = 375 $\mu g \cdot mL^{-1}$) and *S. sclerotiorum* (MIC = 500 $\mu g \cdot mL^{-1}$) compared to other fungal taxa (with MICs ranging from 1000 to 1500 $\mu g \cdot mL^{-1}$). The empty NCs exhibited notable antifungal activity (attributable to the antimicrobial properties of COS and g-C_3N_4), which was lower than that of the extract against *B. cinerea* (MIC = 500 $\mu g \cdot mL^{-1}$) but higher against the remaining phytopathogens, with MICs ranging from 500 to 1000 $\mu g \cdot mL^{-1}$. Regarding the BNP-loaded NCs, a clear enhancement in activity was observed in all cases, resulting in MICs ranging from 187.5 to 375 $\mu g \cdot mL^{-1}$. A comparison of the efficacies of the different treatment*concentration combinations for each of the pathogens is presented in Tables S3–S7.

The aforementioned activity enhancement observed for the BNP-loaded NCs was measured using SFs, all of which were greater than 1 (Table 2), thereby confirming the presence of synergistic action.

Comparisons with conventional fungicides should be approached with caution, considering that plant extracts are complex matrices with several active components, while commercial fungicides typically have specific purity levels and may contain additional substances to enhance their effectiveness. Efficacy values for the three synthetic fungicides used as positive controls are summarized in Table 3. Mancozeb, a dithiocarbamate non-systemic multi-site agricultural fungicide, achieved the complete inhibition of the five fungal taxa even at one-tenth of the manufacturer's recommended dose (200 $\mu g \cdot mL^{-1}$). In contrast, azoxystrobin, a quinone outside inhibitor strobilurin, did not fully arrest the growth of any fungi at the recommended dose of 62,500 $\mu g \cdot mL^{-1}$, with inhibition rates ranging from 32% to 88%. Fosetyl-Al, an organophosphorus systemic fungicide, displayed intermediate efficacy; while it did not inhibit four of the phytopathogens at the recommended dose of 2000 $\mu g \cdot mL^{-1}$ (with inhibition percentages ranging from 65% to 86%), it completely inhibited the growth of *B. cinerea* at this concentration.

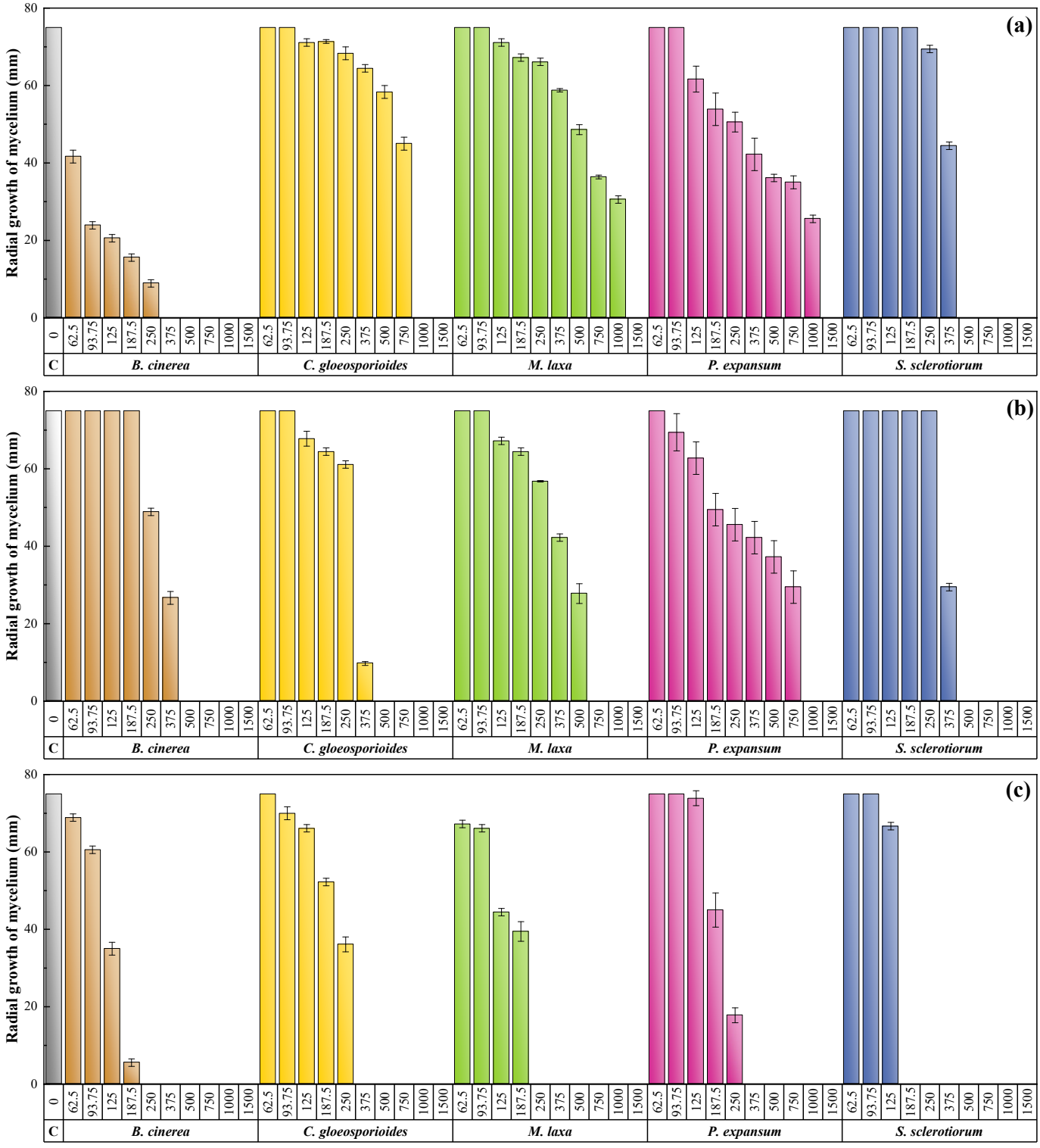

Figure 2. Mycelial growth inhibition achieved with (**a**) the non-encapsulated bioactive natural product (*U. tomentosa* extract), (**b**) the empty COS–HAp–g-C_3N_4 NCs, and (**c**) the COS–HAp–g-C_3N_4 NCs loaded with the BNP against the five fungal pathogens under study at concentrations ranging from 62.5 to 1500 μg·mL^{-1}. Error bars show standard deviations (n = 6). 'C' represents the untreated control.

Table 2. Effective concentration (EC) values (in $\mu g \cdot mL^{-1}$) and synergy factors (SFs) against the five fungal pathogens under study obtained for the non-encapsulated bioactive natural product (*U. tomentosa* extract), the empty COS–HAp–g-C_3N_4 NCs, and the COS–HAp–g-C_3N_4 NCs loaded with the BNP.

Treatment	EC	*B. cinerea*	*C. gloeosporioides*	*M. laxa*	*P. expansum*	*S. sclerotiorum*
U. tomentosa extract	EC_{50}	185.7	786.9	707.9	468.8	392.2
	EC_{90}	482.3	953.3	1368.3	1331.7	476.2
COS–HAp–g-C_3N_4	EC_{50}	306.8	301.2	412.9	472.3	351.8
	EC_{90}	461.9	400.5	673.0	960.1	463.9
COS–HAp–g-C_3N_4–BNP	EC_{50}	123.9	233.9	190.2	200.3	149.3
	EC_{90}	181.2	346.6	236.7	321.2	179.1
SF	EC_{50}	2.13	1.52	2.42	2.35	2.42
	EC_{90}	2.58	1.35	3.26	3.21	2.61

Table 3. In vitro efficacy of three conventional fungicides against the five fungal pathogens under study at the dose recommended by the manufacturer (Rd) and a tenth of the recommended dose (Rd/10).

Commercial Fungicide	Pathogen	Radial Growth of Mycelium (mm)		Inhibition (%)		Ref. **
		Rd/10	Rd *	Rd/10	Rd *	
Azoxystrobin	*B. cinerea*	12	51	84	32	[15]
	C. gloeosporioides	48.9	32.8	34.8	56.3	This work
	M. laxa	33.7	30.3	55	59.6	[37]
	P. expansum	38.9	25.6	48.1	65.9	This work
	S. sclerotiorum	14	9	81.3	88	[38]
Mancozeb	*B. cinerea*	0	0	100	100	[15]
	C. gloeosporioides	0	0	100	100	This work
	M. laxa	0	0	100	100	[37]
	P. expansum	0	0	100	100	This work
	S. sclerotiorum	0	0	100	100	[38]
Fosetyl-Al	*B. cinerea*	38	0	49.3	100	[15]
	C. gloeosporioides	65.6	10.6	12.5	85.9	This work
	M. laxa	72.1	13.3	3.9	82.2	[37]
	P. expansum	67.2	26.1	10.4	65.2	This work
	S. sclerotiorum	75	13.3	0	82.2	[38]

* Rd = 62.5 $mg \cdot mL^{-1}$ of azoxystrobin (250 $mg \cdot mL^{-1}$ for Ortiva®, azoxystrobin 25%), 1.5 $mg \cdot mL^{-1}$ of mancozeb (2 $mg \cdot mL^{-1}$ for Vondozeb®, mancozeb 75%), and 2 $mg \cdot mL^{-1}$ of fosetyl-Al (2.5 $mg \cdot mL^{-1}$ for Fesil®, fosetyl-Al 80%). The control (PDA) exhibited a radial growth of the mycelium of 75 mm. All provided values of mycelial growth are means of three replications. ** Efficacy values against the same isolates previously reported in other studies by our group.

3.2.2. Ex Situ Antifungal Activity

Based on the in vitro results, the BNP-loaded NCs were subsequently employed as a treatment for postharvest protection bioassays on artificially inoculated fruits. Considering that the efficacy of the treatment could be influenced by the absorption and metabolism of the crop protection treatment by the fruit, as well as the variability that may occur between fruits, both the in-vitro-determined MIC and twice the MIC were tested.

The use of the higher treatment dose (twice the MIC) proved to be necessary to achieve high protection, as demonstrated in the results against *B. cinerea* on strawberries (Figure S4), *C. gloeosporioides* on mangoes (Figure S5), *P. expansum* on apples (Figure S6), *M. laxa* on peaches (Figure S7), and *S. sclerotiorum* on kiwifruit (Figure S8), where the efficacy of the treatment at the MIC dose was low. A quantitative comparison based on surface lesion measurements is presented in Table 4, showing LSR values ranging from 25% to 62% at the MIC, compared to 81% to 90% at MIC × 2. Statistically significant differences between the positive controls (fruit intentionally infected with the pathogen and left untreated), the MIC, and the MIC × 2 treatments were found in all cases. Furthermore, in the case of mango, apple, and kiwifruit protection, the lesion size values at MIC × 2 were not statically different from the negative controls (fruit that was neither infected nor treated).

Table 4. Lesion diameter (LD) and lesion size reduction (LSR) in the presence/absence of the NC-based treatment on the different fruits tested in the ex situ postharvest protection bioassays. Negative control refers to untreated fruit without pathogen, and positive control indicates pathogen-inoculated fruit without treatment.

Fruit	Efficacy	Negative Control	Positive Control	COS–HAp–g-C_3N_4–BNP NCs at MIC	COS–HAp–g-C_3N_4–BNP NCs at MIC × 2
Strawberry	LD (mm)	0^{a}	31.8 ± 1.4^{d}	23.8 ± 3.5^{c}	6.1 ± 1.9^{b}
	LSR (%)	100	0	25.2	80.8
Mango	LD (mm)	0^{a}	27.8 ± 1.8^{c}	16.1 ± 2.9^{b}	3.6 ± 1.1^{a}
	LSR (%)	100	0	42.1	87.1
Apple	LD (mm)	0^{a}	37.9 ± 2.9^{c}	14.5 ± 1.6^{b}	4.1 ± 2.1^{a}
	LSR (%)	100	0	61.7	89.2
Peach	LD (mm)	0^{a}	75.0 ± 3.1^{d}	48.2 ± 1.9^{c}	7.5 ± 1.3^{b}
	LSR (%)	100	0	35.7	90
Kiwifruit	LD (mm)	0^{a}	27.5 ± 3.9^{c}	11.4 ± 1.2^{b}	2.8 ± 0.7^{a}
	LSR (%)	100	0	58.5	89.8

The same letters denote non-significant differences at $p < 0.05$. Data were collected at different times after artificial inoculation: 11 days for *B. cinerea* on strawberries, 7 days for *C. gloeosporioides* on mangoes, 15 days for *P. expansum* on apples, 4 days for *M. laxa* on peaches, and 10 days for *S. sclerotiorum* on kiwifruit.

The assessment of internal lesions (shown in Figure S9) supported that the BNP-loaded NC treatment effectively protected the fruit in the exocarp and mesocarp.

4. Discussion

4.1. On the COS–HAp–g-C_3N_4 Assembly

In the literature, FTIR characterization of curcumin-loaded chitosan–HAp NCs confirmed the coverage of chitosan around HAp particles and the hydrogen-bonding interaction between HAp and curcumin [14]. In turn, FTIR spectra of COS–g-C_3N_4 NCs suggested the assembly between COS and *g*-C_3N_4 via the MA cross-linking agent [12]. In the case of COS–HAp–g-C_3N_4 NCs, several possibilities may be considered concerning the linkage between g-C_3N_4 and the COS–HAp pair: (i) via COS through covalent interactions mediated by MA, or through noncovalent and electrostatic interactions via the OH, $–NH_2$, and $–NHCOCH_3$ functional groups of COS [39]; or (ii) via HAp, involving the linkage of g-C_3N_4 to HAp through hydrogen-bonding interactions between PO_4^{3-} of HAp and –OH or $–NH_2$ of g-C_3N_4, as inferred from XPS data by Mohammad et al. [40]. Of these possibilities, the most probable a priori option is the linkage of g-C_3N_4 to the COS–HAp pair via the HAp moiety, resulting in the linkage sequence COS–HAp–g-C_3N_4. This linkage sequence aligns with the relative proportions of each component in the composite, the shared susceptibility of COS and HAp to form nanospheres (g-C_3N_4 is more inclined towards

a lamellar arrangement), and the existing consensus on the stability of the HAp–g-C_3N_4 interaction [41–43].

Concerning the encapsulation of the BNP, given the absence of references to linkages between g-C_3N_4 and natural extracts or EOs in the literature, g-C_3N_4 probably would not play a relevant role. In contrast, this differs for HAp and COS: for instance, HAp has been suggested to contribute to the encapsulation of curcumin in chitosan–HAp NCs via hydrogen bonding [14], while COS would be key to the entrapment of curcumin in chitosan/agarose/g-C_3N_4 nanocomposites and chitosan films incorporated with curcumin-loaded hollow g-C_3N_4 NPs, according to Rajabzadeh-Khosroshahi et al. [13] and Ni et al. [44], respectively. Nonetheless, taking into consideration the larger weight ratio of COS in the COS–HAp–g-C_3N_4 assembly, previous reports on the formation of conjugate complexes between COS and the specific BNP assayed herein (*U. tomentosa* bark extract) [15], and the cationic structure of COS (which lends itself both to being easily linked to anionic crosslinkers [45] and to hydrogen bonding [13]), COS may be put forward as the most probable option.

4.2. Morphological Features of the NCs

The comparison of the morphology of the new NCs with related NCs based on chitosan–HAp, COS–g-C_3N_4, and g-C_3N_4–HAp revealed that only the COS- and HAp-based NCs [12,14] exhibited a spherical morphology, while the g-C_3N_4–HAp composites displayed elongated crystals [46]. Additionally, the different degrees of surface smoothness observed between the empty and filled spheres were previously noted in lignin-based NC systems before and after loading with resveratrol, providing additional evidence of successful BNP encapsulation [47].

4.3. On the Release Mechanism

As in other drug delivery systems, the BNP release from the NCs is primarily expected to be dependent on the COS moiety and its pH-responsive behavior, which is associated with its amine and hydroxyl groups [48]. While a commercial chitosanase (EC 3.2.1.132) was chosen for assessing the release efficiency in this study, it is anticipated that the COS-mediated release in the presence of the phytopathogen would occur due to the presence of organic acids in their secretomes, previously observed for other chitosan-based NCs used for controlling *B. cinerea* and *S. sclerotiorum* [49,50]. It is well-established that many postharvest fungi, such as *B. cinerea*, *Colletotrichum* spp., *Monilinia* spp., *Penicillium* spp., and *S. sclerotiorum* (which were tested herein), can secrete gluconic, oxalic, malic, fumaric, or citric acid [51–53]. As for the actual release mechanism, Hemmati et al. [14] proposed, for chitosan–HAp NCs, that, in the presence of H^+ ions in acidic media, chitosan would swell, causing the release of the drug.

4.4. Comparison of In Vitro Efficacy with Conventional Fungicides

By comparing Tables 2 and 3, it becomes evident that the in vitro efficacy of the COS–HAp–g-C_3N_4 NCs loaded with the BNP (with MIC values of 250, 375, 375, 250, and 187.5 $\mu g \cdot mL^{-1}$ against *B. cinerea*, *C. gloeosporioides*, *P. expansum*, *M. laxa*, and *S. sclerotiorum*, respectively) was lower than that of mancozeb (MIC < 200 $\mu g \cdot mL^{-1}$). However, the BNP-loaded NCs exhibited higher activity than fosetyl-Al and azoxystrobin, both of which have a significant market presence (the global organophosphate pesticides market was estimated at USD 7.06 billion in 2017 [54], and quinone outside inhibitors account for over 30% of the global fungicide market [55]). Their potential replacement with BNP-loaded NCs would offer several advantages, including resistance management by slowing the development of resistance, reducing negative impacts on the environment and non-target organisms, and addressing health concerns.

4.5. Comparison with Other Nanocarriers Tested against the Same Phytopathogens

A direct comparison in terms of activity with NC-based systems reported in the literature for the control of the studied phytopathogens or species belonging to the same genera (summarized in Table S8) is not feasible, as there are no existing examples where the encapsulated active ingredient was a natural extract, as presented in this study.

Based on the encapsulated bioactive product criterion, previously tested systems can be classified into three groups: those with a single, pure product of natural origin; those based on single EOs, combinations of EOs, or their main constituents; and those based on conventional pesticides.

In the first group, berberine hydrochloride (a natural product isolated from the roots and the stem bark of *Berberis* species) [56], curcumin (a polyphenolic compound found in the rhizomes of *Curcuma longa* L.) [57], resveratrol (a phytoalexin produced when plants are attacked by a pathogen found in high quantities on grape skin) [58], and pterostilbene (a natural phenolic compound derived from resveratrol, mostly contained in *Vitis vinifera* L. leaves and grape berries) [59] were tested. Although a direct comparison of concentrations between complex plant extracts and pure substances may not yield meaningful information, it can be observed that concentrations in the range of hundreds of $\mu g \cdot mL^{-1}$, similar to those reported herein (250–750 $\mu g \cdot mL^{-1}$) were required for high inhibition. Considering that comparable efficacies are attained, the direct use of the unrefined plant extract may offer advantages in terms of lower cost, higher efficacy over time (multi-compound products help prevent the development of resistance, as it becomes much harder for the pathogen to adapt to multiple modes of action simultaneously), and applicability against a wide range of pests and diseases (compounds often work synergistically, providing a broad spectrum of activity against various pathogens, while a single purified product may only target specific pests, leaving the crop vulnerable to other threats).

The second group includes EOs from *Azadirachta indica* A.Juss. [60]; *Coriandrum sativum* L. [61]; *Cymbopogon commutatus* (Steud.) Stapf [62]; *Cymbopogon nardus* (L.) Rendle [63]; *Cymbopogon citratus* (DC.) Stapf [64]; *Hyssopus officinalis* L. [65]; *Pistacia atlantica* Desf. [66]; *Salvia officinalis* L. [67]; *Thymus daenensis* Celak. and *Anethum graveolens* L. [68]; *Thymus vulgaris* L. and *Piper betel* L. [69]; *Zataria multiflora* Boiss. [70]; carvacrol and trans-cinnamaldehyde, the main constituents of oregano and cinnamon EOs [71]; D-limonene, the main volatile constituent of citrus peel oil [49]; eugenol, a principal component of the herbal EO from basil [72,73]; and geraniol, a monoterpene alcohol found in the EOs of many plants, including geranium, rose, citronella, lemongrass, lavender, and other aromatic plants [74]. Efficacies largely vary from one study to another, depending on the pathogen and encapsulation system, but concentrations of at least 40 $\mu g \cdot mL^{-1}$ would be required for pure products, and doses in the 20–5000 $\mu g \cdot mL^{-1}$ range would be needed for actual EOs. In this regard, it is worth noting that, while both plant extracts and EOs can be effective at controlling phytopathogens, plant extracts (such as the one discussed in this work) would have some advantages over EOs, including a broader spectrum of activity, less phytotoxicity, easier extraction, and greater stability.

Regarding conventional fungicides, previous studies explored the encapsulation of 1-methylcyclopropene [75], 3-iodo-2-propynyl-N-butylcarbamate [76], 5I-1H-indole [77], azoxystrobin [78], boscalid [79], captan [80], carbendazim [81], dazomet [82], difenoconazole [83], dinotefuran [84], fenhexamid [85], natamycin [86], prochloraz [87–92], and pyraclostrobin [50,93]. While some compounds showed very high efficacies against certain pathogens (e.g., difenoconazole against *C. gloeosporioides*, or carbendazim, fenhexamid, and prochloraz against *S. sclerotiorum*), the activity of the encapsulated extract reported in this work would be comparable to that of captan (with an EC_{50} of 200 $\mu g \cdot mL^{-1}$ against *Colletotrichum capsici* (Syd.) Butler & Bisby), dinotefuran (with 67.1% inhibition at 200 $\mu g \cdot mL^{-1}$), prochloraz (with a 12.7% infection rate at 400 $\mu g \cdot mL^{-1}$ against *Penicillium* spp.), or pyraclostrobin (with 97% inhibition at 200 $\mu g \cdot mL^{-1}$). Advantages associated with their replacement with BNPs have been discussed in the previous section.

In terms of other parameters of the NC-based systems presented in Table S8, it can be observed that the encapsulation efficiencies of polysaccharide-based systems (e.g., β-glucans, β-cyclodextrin, or chitosan) were generally higher than those of inorganic-based systems, with some exceeding 90%, supporting the preference for the former. In this study, the EE for the COS–HAp–g-C_3N_4 NCs (82%) was intermediate compared to previously reported values for *Rubia tinctorum* L. extract encapsulation in COS–g-C_3N_4 NCs (EE = 95–97%) [12] and for curcumin in chitosan–HAp NCs (EE = 75 $\pm$ 4%) [14].

5. Conclusions

The nanocarriers based on COS–HAp–g-C_3N_4, with an average diameter of approximately 250 nm and a loading efficiency of 82%, have proven to be suitable for encapsulating and releasing BNPs with antimicrobial activity, such as cat's claw bark extract. In vitro testing against five fungal taxa responsible for fruit postharvest diseases (grey mold, anthracnose, blue mold, brown rot, and sclerotinia rot), with MIC values ranging from 187.5–375 $\mu g \cdot mL^{-1}$, demonstrated that the NCs outperformed widely used organophosphate and quinone outside inhibitor systemic fungicides. When the BNP-loaded NCs were tested for postharvest protection of fruits (strawberries, mangoes, apples, peaches, and kiwifruit), a higher dose (MIC $\times$ 2) was required to achieve high efficacy, with lesion size reduction values ranging from 81% to 90%. By providing effective postharvest protection against these economically important phytopathogens, the *U. tomentosa*-extract-loaded NCs may help reduce losses in agricultural produce, promote food security, and support environmentally friendly agricultural practices. These findings call for further research to validate the efficacy of the controlled-release nano-delivery system on different genotypes of the selected fruits, on other crops, or against alternative fungal taxa.

6. Patents

The work reported in this manuscript is related to the Spanish patent with application number P202330435 ('Nanomaterial encapsulante formado por g-C_3N_4 y oligómeros de quitosano enlazados a hidroxiapatito, proceso de obtención y usos' which translates as 'Encapsulating nanomaterial formed by g-C_3N_4 and chitosan oligomers linked to hydroxyapatite, process of obtaining and uses'), which was filed on 31 May 2023.

Supplementary Materials: The following supporting information can be downloaded at: https://www.mdpi.com/article/10.3390/agronomy13092189/s1, Figure S1: EDS multi-elemental characterization of the empty nanocarriers and nanocarriers loaded with *U. tomentosa* extract; Figure S2: ATR–FTIR spectra of the empty nanocarriers and nanocarriers loaded with *U. tomentosa* extract; Figure S3: X-ray powder diffraction pattern of the empty nanocarriers and nanocarriers loaded with *U. tomentosa* extract; Figure S4: External lesions caused by *B. cinerea* on strawberries cv. "Fortuna" eleven days after artificial inoculation in the presence/absence of the NC-based treatment; Figure S5: External lesions caused by *C. gloeosporioides* on mangoes cv. "Keitt" seven days after artificial inoculation in the presence/absence of the NC-based treatment; Figure S6: External lesions caused by *P. expansum* on apples cv. "Golden Delicious" fifteen days after artificial inoculation in the presence/absence of the NC-based treatment; Figure S7. External lesions caused by *M. laxa* on peaches cv. "Summer sun" four days after artificial inoculation in the presence/absence of the NC-based treatment; Figure S8: External lesions caused by *S. sclerotiorum* on kiwifruit cv. "Hayward Green" ten days after artificial inoculation in the presence/absence of the NC-based treatment; Figure S9: Internal lesions caused by *C. gloeosporioides* on mangoes, *P. expansum* on apples, *M. laxa* on peaches, and *S. sclerotiorum* on kiwifruit in the presence/absence of the NC-based treatment. Only one replicate per treatment is shown; Table S1: Results of the normality and homoscedasticity tests, along with those of Kruskal–Wallis test, for the mycelial growth inhibition data presented in Figure 2 of the main document; Table S2: Results of the ANOVA, normality, and homoscedasticity tests for the lesion size data presented in Table 4 of the main document; Tables S3–S7: Kruskal–Wallis test and multiple pairwise comparisons using the Conover–Iman procedure for *B. cinerea*, *C. gloeosporioides*, *M. laxa*, *P. expansum*, and *S. sclerotiorum* mycelial growth inhibition values; Table S8: Nanocarriers reported in

the literature for the control of *Botrytis cinerea*, *Colletotrichum* spp., *Monilinia* spp., *Penicillium* spp., and *Sclerotinia sclerotiorum*. Reference [94] is cited in the Supplementary Materials.

Author Contributions: Conceptualization, J.M.-G. and P.M.-R.; methodology, J.L.M.-R. and J.M.-G.; validation, J.L.M.-R.; formal analysis, E.S.-H., J.M.-G. and P.M.-R.; investigation, A.S.-A., E.S.-H., L.B.-D., J.L.M.-R., J.M.-G. and P.M.-R.; resources, J.M.-G.; writing—original draft preparation, A.S.-A., E.S.-H., L.B.-D., J.L.M.-R., J.M.-G. and P.M.-R.; writing—review and editing, E.S.-H., L.B.-D., J.M.-G. and P.M.-R.; visualization, A.S.-A. and E.S.-H.; supervision, P.M.-R.; project administration, E.S.-H. and J.M.-G.; funding acquisition, E.S.-H. and J.M.-G. All authors have read and agreed to the published version of the manuscript.

Funding: This research was funded by Fundación General de la Universidad de Valladolid through the project APLICADRON.

Data Availability Statement: The data presented in this study are available upon request from the corresponding author. The data are not publicly available due to their relevance to an ongoing Ph.D. thesis.

Acknowledgments: The authors thank the Fundación General de la Universidad de Valladolid for funding the patent through the 'Prometeo' program.

Conflicts of Interest: The authors declare no conflict of interest. The funders had no role in the design of the study; in the collection, analyses, or interpretation of data; in the writing of the manuscript; or in the decision to publish the results.

References

1. Khizar, S.; Alrushaid, N.; Alam Khan, F.; Zine, N.; Jaffrezic-Renault, N.; Errachid, A.; Elaissari, A. Nanocarriers based novel and effective drug delivery system. *Int. J. Pharm.* **2023**, *632*, 122570. [CrossRef]
2. Nagaraj, S.; Manivannan, S.; Narayan, S. Potent antifungal agents and use of nanocarriers to improve delivery to the infected site: A systematic review. *J. Basic. Microbiol.* **2021**, *61*, 849–873. [CrossRef] [PubMed]
3. Ojha, S.; Singh, D.; Sett, A.; Chetia, H.; Kabiraj, D.; Bora, U. Nanotechnology in crop protection. In *Nanomaterials in Plants, Algae, and Microorganisms*; Tripathi, D.K., Ahmad, P., Sharma, S., Chauhan, D.K., Dubey, N.K., Eds.; Academic Press: London, UK, 2018; pp. 345–391. [CrossRef]
4. Xiao, D.; Wu, H.; Zhang, Y.; Kang, J.; Dong, A.; Liang, W. Advances in stimuli-responsive systems for pesticides delivery: Recent efforts and future outlook. *J. Control. Release* **2022**, *352*, 288–312. [CrossRef] [PubMed]
5. Bahrami, A.; Delshadi, R.; Assadpour, E.; Jafari, S.M.; Williams, L. Antimicrobial-loaded nanocarriers for food packaging applications. *Adv. Colloid. Interface Sci.* **2020**, *278*, 102140. [CrossRef]
6. Pinto, T.V.; Silva, C.A.; Siquenique, S.; Learmonth, D.A. Micro- and nanocarriers for encapsulation of biological plant protection agents: A systematic literature review. *ACS Agric. Sci. Technol.* **2022**, *2*, 838–857. [CrossRef]
7. Tao, R.; You, C.; Qu, Q.; Zhang, X.; Deng, Y.; Ma, W.; Huang, C. Recent advances in the design of controlled- and sustained-release micro/nanocarriers of pesticide. *Environ. Sci. Nano* **2023**, *10*, 351–371. [CrossRef]
8. Zhou, J.; Liu, G.; Guo, Z.; Wang, M.; Qi, C.; Chen, G.; Huang, X.; Yan, S.; Xu, D. Stimuli-responsive pesticide carriers based on porous nanomaterials: A review. *Chem. Eng. J.* **2023**, *455*, 140167. [CrossRef]
9. Tleuova, A.B.; Wielogorska, E.; Talluri, V.S.S.L.P.; Štěpánek, F.; Elliott, C.T.; Grigoriev, D.O. Recent advances and remaining barriers to producing novel formulations of fungicides for safe and sustainable agriculture. *J. Control. Release* **2020**, *326*, 468–481. [CrossRef]
10. Fincheira, P.; Hoffmann, N.; Tortella, G.; Ruiz, A.; Cornejo, P.; Diez, M.C.; Seabra, A.B.; Benavides-Mendoza, A.; Rubilar, O. Eco-efficient systems based on nanocarriers for the controlled release of fertilizers and pesticides: Toward smart agriculture. *Nanomaterials* **2023**, *13*, 1978. [CrossRef]
11. Yang, Y.; Aghbashlo, M.; Gupta, V.K.; Amiri, H.; Pan, J.; Tabatabaei, M.; Rajaei, A. Chitosan nanocarriers containing essential oils as a green strategy to improve the functional properties of chitosan: A review. *Int. J. Biol. Macromol.* **2023**, *236*, 123954. [CrossRef]
12. Santiago-Aliste, A.; Sánchez-Hernández, E.; Langa-Lomba, N.; González-García, V.; Casanova-Gascón, J.; Martín-Gil, J.; Martín-Ramos, P. Multifunctional nanocarriers based on chitosan oligomers and graphitic carbon nitride assembly. *Materials* **2022**, *15*, 8981. [CrossRef] [PubMed]
13. Rajabzadeh-Khosroshahi, M.; Pourmadadi, M.; Yazdian, F.; Rashedi, H.; Navaei-Nigjeh, M.; Rasekh, B. Chitosan/agarose/graphitic carbon nitride nanocomposite as an efficient pH-sensitive drug delivery system for anticancer curcumin releasing. *J. Drug. Deliv. Sci. Technol.* **2022**, *74*, 103443. [CrossRef]
14. Hemmati, K.; Ahmadi Nasab, N.; Hesaraki, S.; Nezafati, N. In vitro evaluation of curcumin-loaded chitosan-coated hydroxyapatite nanocarriers as a potential system for effective treatment of cancer. *J. Biomater. Sci. Polym. Ed.* **2021**, *32*, 1267–1287. [CrossRef] [PubMed]

15. Sánchez-Hernández, E.; Martín-Ramos, P.; Martín-Gil, J.; Santiago-Aliste, A.; Hernández-Navarro, S.; Oliveira, R.; González-García, V. Bark extract of *Uncaria tomentosa* L. for the control of strawberry phytopathogens. *Horticulturae* **2022**, *8*, 672. [CrossRef]
16. Dean, R.; Van Kan, J.A.L.; Pretorius, Z.A.; Hammond-Kosack, K.E.; Di Pietro, A.; Spanu, P.D.; Rudd, J.J.; Dickman, M.; Kahmann, R.; Ellis, J.; et al. The top 10 fungal pathogens in molecular plant pathology. *Mol. Plant. Pathol.* **2012**, *13*, 414–430. [CrossRef] [PubMed]
17. Peralta-Ruiz, Y.; Rossi, C.; Grande-Tovar, C.D.; Chaves-López, C. Green management of postharvest anthracnose caused by *Colletotrichum gloeosporioides*. *J. Fungi* **2023**, *9*, 623. [CrossRef]
18. Wang, K.; Ngea, G.L.N.; Godana, E.A.; Shi, Y.; Lanhuang, B.; Zhang, X.; Zhao, L.; Yang, Q.; Wang, S.; Zhang, H. Recent advances in *Penicillium expansum* infection mechanisms and current methods in controlling *P. expansum* in postharvest apples. *Crit. Rev. Food Sci. Nutr.* **2021**, *63*, 2598–2611. [CrossRef]
19. Rungjindamai, N.; Jeffries, P.; Xu, X.-M. Epidemiology and management of brown rot on stone fruit caused by *Monilinia laxa*. *Eur. J. Plant. Pathol.* **2014**, *140*, 1–17. [CrossRef]
20. Obi, V.I.; Barriuso, J.J.; Gogorcena, Y. Peach brown rot: Still in search of an ideal management option. *Agriculture* **2018**, *8*, 125. [CrossRef]
21. Kim, G.H.; Koh, Y.J. Diagnosis and integrated management of major fungal fruit rots on kiwifruit in Korea. *Res. Plant. Dis.* **2018**, *24*, 113–122. [CrossRef]
22. Lee, J.H.; Kwon, Y.H.; Kwack, Y.-B.; Kwak, Y.-S. Report of postharvest rot of kiwifruit in Korea caused by *Sclerotinia sclerotiorum*. *Int. J. Food Microbiol.* **2015**, *206*, 81–83. [CrossRef]
23. Santos-Moriano, P.; Fernandez-Arrojo, L.; Mengibar, M.; Belmonte-Reche, E.; Peñalver, P.; Acosta, F.N.; Ballesteros, A.O.; Morales, J.C.; Kidibule, P.; Fernandez-Lobato, M.; et al. Enzymatic production of fully deacetylated chitooligosaccharides and their neuroprotective and anti-inflammatory properties. *Biocatal. Biotransform.* **2017**, *36*, 57–67. [CrossRef]
24. Dante, R.C.; Martín-Ramos, P.; Sánchez-Arévalo, F.M.; Huerta, L.; Bizarro, M.; Navas-Gracia, L.M.; Martín-Gil, J. Synthesis of crumpled nanosheets of polymeric carbon nitride from melamine cyanurate. *J. Solid. State Chem.* **2013**, *201*, 153–163. [CrossRef]
25. Kim, W.; Saito, F. Sonochemical synthesis of hydroxyapatite from H_3PO_4 solution with $Ca(OH)_2$. *Ultrason. Sonochem.* **2001**, *8*, 85–88. [CrossRef]
26. Gupta, B.; Gupta, A.K. Photocatalytic performance of 3D engineered chitosan hydrogels embedded with sulfur-doped C_3N_4/ZnO nanoparticles for Ciprofloxacin removal: Degradation and mechanistic pathways. *Int. J. Biol. Macromol.* **2022**, *198*, 87–100. [CrossRef]
27. Fischer, J.; Beckers, S.J.; Yiamsawas, D.; Thines, E.; Landfester, K.; Wurm, F.R. Targeted drug delivery in plants: Enzyme-responsive lignin nanocarriers for the curative treatment of the worldwide grapevine trunk disease Esca. *Adv. Sci.* **2019**, *6*, 1802315. [CrossRef] [PubMed]
28. Krizsán, K.; Szókán, G.; Toth, Z.A.; Hollósy, F.; László, M.; Khlafulla, A. HPLC analysis of anthraquinone derivatives in madder root (*Rubia tinctorum*) and its cell cultures. *J. Liq. Chromatogr. Relat. Technol.* **2006**, *19*, 2295–2314. [CrossRef]
29. Tiunov, I.A.; Gorbachevskyy, M.V.; Kopitsyn, D.S.; Kotelev, M.S.; Ivanov, E.V.; Vinokurov, V.A.; Novikov, A.A. Synthesis of large uniform gold and core–shell gold–silver nanoparticles: Effect of temperature control. *Russ. J. Phys. Chem. A.* **2016**, *90*, 152–157. [CrossRef]
30. Arendrup, M.C.; Cuenca-Estrella, M.; Lass-Flörl, C.; Hope, W. EUCAST technical note on the EUCAST definitive document EDef 7.2: Method for the determination of broth dilution minimum inhibitory concentrations of antifungal agents for yeasts EDef 7.2 (EUCAST-AFST). *Clin. Microbiol. Infect.* **2012**, *18*, E246–E247. [CrossRef]
31. Levy, Y.; Benderly, M.; Cohen, Y.; Gisi, U.; Bassand, D. The joint action of fungicides in mixtures: Comparison of two methods for synergy calculation. *EPPO Bull.* **1986**, *16*, 651–657. [CrossRef]
32. Sánchez-Hernández, E.; González-García, V.; Correa-Guimarães, A.; Casanova-Gascón, J.; Martín-Gil, J.; Martín-Ramos, P. Phytochemical profile and activity against *Fusarium* species of *Tamarix gallica* bark aqueous ammonia extract. *Agronomy* **2023**, *13*, 496. [CrossRef]
33. Sánchez-Hernández, E.; Álvarez-Martínez, J.; González-García, V.; Casanova-Gascón, J.; Martín-Gil, J.; Martín-Ramos, P. *Helichrysum stoechas* (L.) Moench inflorescence extract for tomato disease management. *Molecules* **2023**, *28*, 5861. [CrossRef]
34. Sadeghi, R.; Etemad, S.G.; Keshavarzi, E.; Haghshenasfard, M. Investigation of alumina nanofluid stability by UV–vis spectrum. *Microfluid. Nanofluidics* **2015**, *18*, 1023–1030. [CrossRef]
35. Jaworska, M.; Sakurai, K.; Gaudon, P.; Guibal, E. Influence of chitosan characteristics on polymer properties. I: Crystallographic properties. *Polym. Int.* **2003**, *52*, 198–205. [CrossRef]
36. Sierra, M.; Borges, E.; Esparza, P.; Méndez-Ramos, J.; Martín-Gil, J.; Martín-Ramos, P. Photocatalytic activities of coke carbon/g-C_3N_4 and Bi metal/Bi mixed oxides/g-C_3N_4 nanohybrids for the degradation of pollutants in wastewater. *Sci. Technol. Adv. Mater.* **2016**, *17*, 659–668. [CrossRef] [PubMed]
37. Sánchez-Hernández, E.; González-García, V.; Casanova-Gascón, J.; Barriuso-Vargas, J.J.; Balduque-Gil, J.; Lorenzo-Vidal, B.; Martín-Gil, J.; Martín-Ramos, P. Valorization of *Quercus suber* L. bark as a source of phytochemicals with antimicrobial activity against apple tree diseases. *Plants* **2022**, *11*, 3415. [CrossRef] [PubMed]
38. Sánchez-Hernández, E.; Martín-Ramos, P.; Navas Gracia, L.M.; Martín-Gil, J.; Garcés-Claver, A.; Flores-León, A.; González-García, V. *Armeria maritima* (Mill.) Willd. flower hydromethanolic extract for Cucurbitaceae fungal diseases control. *Molecules* **2023**, *28*, 3730. [CrossRef]

39. Li, H.; Li, F.; Wang, Z.; Jiao, Y.; Liu, Y.; Wang, P.; Zhang, X.; Qin, X.; Dai, Y.; Huang, B. Fabrication of carbon bridged g-C_3N_4 through supramolecular self-assembly for enhanced photocatalytic hydrogen evolution. *Appl. Catal. B. Environ.* **2018**, *229*, 114–120. [CrossRef]
40. Mohammad, I.; Jeshurun, A.; Ponnusamy, P.; Reddy, B.M. Mesoporous graphitic carbon nitride/hydroxyapatite (g-C_3N_4/HAp) nanocomposites for highly efficient photocatalytic degradation of rhodamine B dye. *Mater. Today Commun.* **2022**, *33*, 104788. [CrossRef]
41. Xu, T.; Zou, R.; Lei, X.; Qi, X.; Wu, Q.; Yao, W.; Xu, Q. New and stable g-C_3N_4/HAp composites as highly efficient photocatalysts for tetracycline fast degradation. *Appl. Catal. B. Environ.* **2019**, *245*, 662–671. [CrossRef]
42. Saranya, A.; Vishwa Priya, U.; Varun Prasath, P.; Sankara Narayanan, T.S.N.; Ravichandran, K. Photochemical degradation of Congo red using magnesium doped hydroxyapatite-graphitic carbon nitride composite. *Mater. Today Proc.* **2022**, *68*, 1–6. [CrossRef]
43. Vishwa Priya, U.; Saranya, A.; Varun Prasath, P.; Ravichandran, K. Investigation of in vitro biological studies on Fe doped hydroxyapatite-graphitic carbon nitride composite. *Mater. Today Proc.* **2022**, *68*, 43–49. [CrossRef]
44. Ni, Y.; Nie, H.; Wang, J.; Lin, J.; Wang, Q.; Sun, J.; Zhang, W.; Wang, J. Enhanced functional properties of chitosan films incorporated with curcumin-loaded hollow graphitic carbon nitride nanoparticles for bananas preservation. *Food Chem.* **2022**, *366*, 130539. [CrossRef]
45. Chuah, L.H.; Billa, N.; Roberts, C.J.; Burley, J.C.; Manickam, S. Curcumin-containing chitosan nanoparticles as a potential mucoadhesive delivery system to the colon. *Pharm. Dev. Technol.* **2011**, *18*, 591–599. [CrossRef] [PubMed]
46. Vishwapriya, U. Hydroxyapatite-graphitic carbon nitride based composites: Synthesis, characterization, and evaluation of bioactivity. *ECS Trans.* **2022**, *107*, 16769–16778. [CrossRef]
47. Dai, L.; Liu, R.; Hu, L.-Q.; Zou, Z.-F.; Si, C.-L. Lignin nanoparticle as a novel green carrier for the efficient delivery of resveratrol. *ACS Sustain. Chem. Eng.* **2017**, *5*, 8241–8249. [CrossRef]
48. Xing, L.; Fan, Y.-T.; Shen, L.-J.; Yang, C.-X.; Liu, X.-Y.; Ma, Y.-N.; Qi, L.-Y.; Cho, K.-H.; Cho, C.-S.; Jiang, H.-L. pH-sensitive and specific ligand-conjugated chitosan nanogels for efficient drug delivery. *Int. J. Biol. Macromol.* **2019**, *141*, 85–97. [CrossRef]
49. Vega-Vásquez, P.; Mosier, N.S.; Irudayaraj, J. Nanovaccine for plants from organic waste: D-limonene-loaded chitosan nanocarriers protect plants against *Botrytis cinerea*. *ACS Sustain. Chem. Eng.* **2021**, *9*, 9903–9914. [CrossRef]
50. Xu, L.; Cao, L.-D.; Li, F.-M.; Wang, X.-J.; Huang, Q.-L. Utilization of chitosan-lactide copolymer nanoparticles as controlled release pesticide carrier for pyraclostrobin against *Colletotrichum gossypii* Southw. *J. Dispers. Sci. Technol.* **2014**, *35*, 544–550. [CrossRef]
51. Jiao, W.; Liu, X.; Li, Y.; Li, B.; Du, Y.; Zhang, Z.; Chen, Q.; Fu, M. Organic acid, a virulence factor for pathogenic fungi, causing postharvest decay in fruits. *Mol. Plant. Pathol.* **2021**, *23*, 304–312. [CrossRef]
52. De Cal, A.; Sandín-España, P.; Martinez, F.; Egüen, B.; Chien-Ming, C.; Lee, M.H.; Melgarejo, P.; Prusky, D. Role of gluconic acid and pH modulation in virulence of *Monilinia fructicola* on peach fruit. *Postharvest Biol. Technol.* **2013**, *86*, 418–423. [CrossRef]
53. Reveglia, P.; Agudo-Jurado, F.J.; Barilli, E.; Masi, M.; Evidente, A.; Rubiales, D. Uncovering phytotoxic compounds produced by *Colletotrichum* spp. involved in legume diseases using an OSMAC–metabolomics approach. *J. Fungi* **2023**, *9*, 610. [CrossRef]
54. Paidi, M.K.; Satapute, P.; Haider, M.S.; Udikeri, S.S.; Ramachandra, Y.L.; Vo, D.-V.N.; Govarthanan, M.; Jogaiah, S. Mitigation of organophosphorus insecticides from environment: Residual detoxification by bioweapon catalytic scavengers. *Environ. Res.* **2021**, *200*, 111368. [CrossRef]
55. Duan, Y.; Lu, F.; Zhou, Z.; Zhao, H.; Zhang, J.; Mao, Y.; Li, M.; Wang, J.; Zhou, M. Quinone outside inhibitors affect DON biosynthesis, mitochondrial structure and toxisome formation in *Fusarium graminearum*. *J. Hazard. Mater.* **2020**, *398*, 122908. [CrossRef] [PubMed]
56. Wang, C.-Y.; Lou, X.-Y.; Cai, Z.; Zhang, M.-Z.; Jia, C.; Qin, J.-C.; Yang, Y.-W. Supramolecular nanoplatform based on mesoporous silica nanocarriers and pillararene nanogates for fungus control. *ACS Appl. Mater. Interfaces* **2021**, *13*, 32295–32306. [CrossRef] [PubMed]
57. Bhawana; Basniwal, R.K.; Buttar, H.S.; Jain, V.K.; Jain, N. Curcumin nanoparticles: Preparation, characterization, and antimicrobial study. *J. Agric. Food. Chem.* **2011**, *59*, 2056–2061. [CrossRef]
58. Salgado, M.; Rodríguez-Rojo, S.; Alves-Santos, F.M.; Cocero, M.J. Encapsulation of resveratrol on lecithin and β-glucans to enhance its action against *Botrytis cinerea*. *J. Food Eng.* **2015**, *165*, 13–21. [CrossRef]
59. De Angelis, G.; Simonetti, G.; Chronopoulou, L.; Orekhova, A.; Badiali, C.; Petruccelli, V.; Portoghesi, F.; D'Angeli, S.; Brasili, E.; Pasqua, G.; et al. A novel approach to control *Botrytis cinerea* fungal infections: Uptake and biological activity of antifungals encapsulated in nanoparticle based vectors. *Sci. Rep.* **2022**, *12*, 7989. [CrossRef]
60. de Castro e Silva, P.; Pereira, L.A.S.; de Rezende, É.M.; dos Reis, M.V.; Lago, A.M.T.; Carvalho, G.R.; Paiva, R.; Oliveira, J.E.; Marconcini, J.M. Production and efficacy of neem nanoemulsion in the control of *Aspergillus flavus* and *Penicillium citrinum* in soybean seeds. *Eur. J. Plant. Pathol.* **2019**, *155*, 1105–1116. [CrossRef]
61. Das, S.; Singh, V.K.; Dwivedy, A.K.; Chaudhari, A.K.; Upadhyay, N.; Singh, P.; Sharma, S.; Dubey, N.K. Encapsulation in chitosan-based nanomatrix as an efficient green technology to boost the antimicrobial, antioxidant and in situ efficacy of *Coriandrum sativum* essential oil. *Int. J. Biol. Macromol.* **2019**, *133*, 294–305. [CrossRef]
62. Soltanzadeh, M.; Peighambardoust, S.H.; Ghanbarzadeh, B.; Mohammadi, M.; Lorenzo, J.M. Chitosan nanoparticles encapsulating lemongrass (*Cymbopogon commutatus*) essential oil: Physicochemical, structural, antimicrobial and in-vitro release properties. *Int. J. Biol. Macromol.* **2021**, *192*, 1084–1097. [CrossRef] [PubMed]

63. Prasad, J.; Das, S.; Maurya, A.; Jain, S.K.; Dwivedy, A.K. Synthesis, characterization and in situ bioefficacy evaluation of *Cymbopogon nardus* essential oil impregnated chitosan nanoemulsion against fungal infestation and aflatoxin B1 contamination in food system. *Int. J. Biol. Macromol.* **2022**, *205*, 240–252. [CrossRef]
64. Tofiño-Rivera, A.P.; Castro-Amaris, G.; Casierra-Posada, F. Effectiveness of *Cymbopogon citratus* oil encapsulated in chitosan on *Colletotrichum gloeosporioides* isolated from *Capsicum annuum*. *Molecules* **2020**, *25*, 4447. [CrossRef]
65. Hadidi, M.; Motamedzadegan, A.; Jelyani, A.Z.; Khashadeh, S. Nanoencapsulation of hyssop essential oil in chitosan-pea protein isolate nano-complex. *LWT* **2021**, *144*, 111254. [CrossRef]
66. Hesami, G.; Darvishi, S.; Zarei, M.; Hadidi, M. Fabrication of chitosan nanoparticles incorporated with *Pistacia atlantica* subsp. kurdica hulls' essential oil as a potential antifungal preservative against strawberry grey mould. *Int. J. Food Sci. Technol.* **2021**, *56*, 4215–4223. [CrossRef]
67. Erarslan, A.; Karakas, C.Y.; Bozkurt, F.; Sagdic, O. Enhanced antifungal activity of electrosprayed poly (vinyl alcohol)/chitosan nanospheres loaded with sage essential oil on the viability of *Aspergillus niger* and *Botrytis cinerea*. *ChemistrySelect* **2023**, *8*, e202300296. [CrossRef]
68. Weisany, W.; Samadi, S.; Amini, J.; Hossaini, S.; Yousefi, S.; Maggi, F. Enhancement of the antifungal activity of thyme and dill essential oils against *Colletotrichum nymphaeae* by nano-encapsulation with copper NPs. *Ind. Crops Prod.* **2019**, *132*, 213–225. [CrossRef]
69. Gundewadi, G.; Rudra, S.G.; Gogoi, R.; Banerjee, T.; Singh, S.K.; Dhakate, S.; Gupta, A. Electrospun essential oil encapsulated nanofibers for the management of anthracnose disease in sapota. *Ind. Crops Prod.* **2021**, *170*, 113727. [CrossRef]
70. Mohammadi, A.; Hashemi, M.; Hosseini, S.M. Nanoencapsulation of *Zataria multiflora* essential oil preparation and characterization with enhanced *antifungal activity for controlling Botrytis cinerea*, the causal agent of gray mould disease. *Innov. Food Sci. Emerg. Technol.* **2015**, *28*, 73–80. [CrossRef]
71. Canales, D.; Montoille, L.; Rivas, L.M.; Ortiz, J.A.; Yañez, S.M.; Rabagliati, F.M.; Ulloa, M.T.; Alvarez, E.; Zapata, P.A. Fungicides films of low-density polyethylene (LDPE)/inclusion complexes (carvacrol and cinnamaldehyde) against *Botrytis cinerea*. *Coatings* **2019**, *9*, 795. [CrossRef]
72. Wang, C.Y.; Jia, C.; Zhang, M.Z.; Yang, S.; Qin, J.C.; Yang, Y.W. A lesion microenvironment-responsive fungicide nanoplatform for crop disease prevention and control. *Adv. Healthc. Mater.* **2022**, *11*, 2102617. [CrossRef]
73. Xue, Y.; Zhou, S.; Fan, C.; Du, Q.; Jin, P. Enhanced antifungal activities of eugenol-entrapped casein nanoparticles against anthracnose in postharvest fruits. *Nanomaterials* **2019**, *9*, 1777. [CrossRef] [PubMed]
74. Tryfon, P.; Kamou, N.N.; Pavlou, A.; Mourdikoudis, S.; Menkissoglu-Spiroudi, U.; Dendrinou-Samara, C. Nanocapsules of ZnO nanorods and geraniol as a novel mean for the effective control of *Botrytis cinerea* in tomato and cucumber plants. *Plants* **2023**, *12*, 1074. [CrossRef]
75. Seglie, L.; Spadaro, D.; Trotta, F.; Devecchi, M.; Gullino, M.L.; Scariot, V. Use of 1-methylcylopropene in cyclodextrin-based nanosponges to control grey mould caused by *Botrytis cinerea* on *Dianthus caryophyllus* cut flowers. *Postharvest Biol. Technol.* **2012**, *64*, 55–57. [CrossRef]
76. Raimond, L.; Halbus, A.F.; Athab, Z.H.; Paunov, V.N. Antimould action of Ziram and IPBC loaded in functionalised nanogels against *Aspergillus niger* and *Penicillium chrysogenum*. *Mater. Adv.* **2022**, *3*, 8178–8192. [CrossRef]
77. Raj, V.; Raorane, C.J.; Lee, J.-H.; Lee, J. Appraisal of chitosan-gum arabic-coated bipolymeric nanocarriers for efficient dye removal and eradication of the plant pathogen *Botrytis cinerea*. *ACS Appl. Mater. Interfaces* **2021**, *13*, 47354–47370. [CrossRef]
78. Yao, J.; Cui, B.; Zhao, X.; Zhi, H.; Zeng, Z.; Wang, Y.; Sun, C.; Liu, G.; Gao, J.; Cui, H. Antagonistic effect of azoxystrobin poly (lactic acid) microspheres with controllable particle size on *Colletotrichum higginsianum* Sacc. *Nanomaterials* **2018**, *8*, 857. [CrossRef] [PubMed]
79. Zhang, X.; Tang, X.; Zhao, C.; Yuan, Z.; Zhang, D.; Zhao, H.; Yang, N.; Guo, K.; He, Y.; He, Y.; et al. A pH-responsive MOF for site-specific delivery of fungicide to control citrus disease of *Botrytis cinerea*. *Chem. Eng. J.* **2022**, *431*, 133351. [CrossRef]
80. Sharma, S.; Singh, B.; Bindra, P.; Panneerselvam, P.; Dwivedi, N.; Senapati, A.; Adholeya, A.; Shanmugam, V. Triple-smart eco-friendly chili anthracnose control agro-nanocarrier. *ACS Appl. Mater. Interfaces* **2021**, *13*, 9143–9155. [CrossRef]
81. Huang, Y.; Yang, Y.; Liang, B.; Lu, S.; Yuan, X.; Jia, Z.; Liu, J.; Liu, Y. Green nanopesticide: pH-responsive eco-friendly pillar[5]arene-modified selenium nanoparticles for smart delivery of carbendazim to suppress *Sclerotinia* diseases. *ACS Appl. Mater. Interfaces* **2023**, *15*, 16448–16459. [CrossRef] [PubMed]
82. Ren, L.; Zhao, J.; Li, W.; Li, Q.; Zhang, D.; Fang, W.; Yan, D.; Li, Y.; Wang, Q.; Jin, X.; et al. Site-specific controlled-release imidazolate framework-8 for dazomet smart delivery to improve the effective utilization rate and reduce biotoxicity. *J. Agric. Food. Chem.* **2022**, *70*, 5993–6005. [CrossRef] [PubMed]
83. Liang, W.; Zhang, J.; Wurm, F.R.; Wang, R.; Cheng, J.; Xie, Z.; Li, X.; Zhao, J. Lignin-based non-crosslinked nanocarriers: A promising delivery system of pesticide for development of sustainable agriculture. *Int. J. Biol. Macromol.* **2022**, *220*, 472–481. [CrossRef]
84. Hong, T.; Wan, M.; Lv, S.; Peng, L.; Zhao, Y. Metal-phenolic coated rod-like silica nanocarriers with pH responsiveness for pesticide delivery. *Colloids Surf. A Physicochem. Eng. Asp.* **2023**, *662*, 130989. [CrossRef]
85. Tang, G.; Tian, Y.; Niu, J.; Tang, J.; Yang, J.; Gao, Y.; Chen, X.; Li, X.; Wang, H.; Cao, Y. Development of carrier-free self-assembled nanoparticles based on fenhexamid and polyhexamethylene biguanide for sustainable plant disease management. *Green Chem.* **2021**, *23*, 2531–2540. [CrossRef]

86. Xu, X.; Peng, X.; Huan, C.; Chen, J.; Meng, Y.; Fang, S. Development of natamycin-loaded zein-casein composite nanoparticles by a pH-driven method and application to postharvest fungal control on peach against *Monilinia fructicola*. *Food Chem.* **2023**, *404*, 134659. [CrossRef] [PubMed]
87. Liang, Y.; Fan, C.; Dong, H.; Zhang, W.; Tang, G.; Yang, J.; Jiang, N.; Cao, Y. Preparation of MSNs-chitosan@prochloraz nanoparticles for reducing toxicity and improving release properties of prochloraz. *ACS Sustain. Chem. Eng.* **2018**, *6*, 10211–10220. [CrossRef]
88. Gao, Y.; Liang, Y.; Dong, H.; Niu, J.; Tang, J.; Yang, J.; Tang, G.; Zhou, Z.; Tang, R.; Shi, X.; et al. A bioresponsive system based on mesoporous organosilica nanoparticles for smart delivery of fungicide in response to pathogen presence. *ACS Sustain. Chem. Eng.* **2020**, *8*, 5716–5723. [CrossRef]
89. Xiao, D.; Cheng, J.; Liang, W.; Sun, L.; Zhao, J. Metal-phenolic coated and prochloraz-loaded calcium carbonate carriers with pH responsiveness for environmentally-safe fungicide delivery. *Chem. Eng. J.* **2021**, *418*, 129274. [CrossRef]
90. Shi, L.; Liang, Q.; Zang, Q.; Lv, Z.; Meng, X.; Feng, J. Construction of prochloraz-loaded hollow mesoporous silica nanoparticles coated with metal–phenolic networks for precise release and improved biosafety of pesticides. *Nanomaterials* **2022**, *12*, 2885. [CrossRef]
91. Yang, J.; Gao, Y.; Zhou, Z.; Tang, J.; Tang, G.; Niu, J.; Chen, X.; Tian, Y.; Li, Y.; Cao, Y. A simple and green preparation process for PRO@PIL-PHS-PEC microcapsules by using phosphonium ionic liquid as a multifunctional additive. *Chem. Eng. J.* **2021**, *424*, 130371. [CrossRef]
92. Liang, W.; Xie, Z.; Cheng, J.; Xiao, D.; Xiong, Q.; Wang, Q.; Zhao, J.; Gui, W. A light-triggered pH-responsive metal–organic framework for smart delivery of fungicide to control *Sclerotinia* diseases of oilseed rape. *ACS Nano* **2021**, *15*, 6987–6997. [CrossRef] [PubMed]
93. Peng, F.; Wang, X.; Zhang, W.; Shi, X.; Cheng, C.; Hou, W.; Lin, X.; Xiao, X.; Li, J. Nanopesticide formulation from pyraclostrobin and graphene oxide as a nanocarrier and application in controlling plant fungal pathogens. *Nanomaterials* **2022**, *12*, 1112. [CrossRef] [PubMed]
94. Niu, X.; Lin, L.; Liu, L.; Wang, H. Preparation of a novel glucose oxidase-N-succinyl chitosan nanospheres and its antifungal mechanism of action against *Colletotrichum gloeosporioides*. *Int. J. Biol. Macromol.* **2023**, *228*, 681–691. [CrossRef] [PubMed]